52nd IEEE Conference on Decision and Control
December 10-13, 2013. Florence, Italy

Load-Frequency Control, Economic Dispatch and Unit Commitment in Smart Microgrids based on Hierarchical Model Predictive Control

Felix Berkel, Daniel Görges, and Steven Liu

Abstract— **This paper presents an energy management system for smart microgrids (MGs) based on hierarchical model predictive control (HiMPC). The HiMPC comprises two levels. On the lower level load-frequency control is realized on a short time scale while on the upper level economic dispatch and unit commitment are implemented on a long time scale. HiMPC allows integrating these functionalities over different time scales while regarding constraints (e.g. power ratings) and predictions (e.g. on renewable generation and load) as well as rejecting disturbances (e.g. due to volatile renewable generation) based on a systematic model- and optimization-based design. The HiMPC problem is formulated as a mixed-integer linear program which can be solved efficiently using standard solvers. The energy management system is evaluated for a smart MG of a company with a focus on grid integration of electric vehicles.**

I. Introduction

Power systems are currently in an unprecedented change as generation shifts from few large centralized conventional generation units to many small decentralized renewable ones. For example in Germany the renewable electricity generation has increased from 3.1 % in 1990 to 17.0 % in 2010 [1] and is projected to further increase to 38.6 % in 2020 [2]. Similar activities have started all over the world. The decentralization and volatility of renewable generation units pose substantial challenges on power system operation and control.

Power system operation and control comprises several tasks [3], namely load-frequency control (LFC) for the regulation of the frequency, optimal power flow (OPF) for an economic operation of the transmission and distribution grid, economic dispatch (ED) for an economic operation of the generation units and unit commitment (UC) for an economic selection of the generation units. These tasks must be solved on different time scales which is traditionally realized using hierarchical control. LFC is partitioned into primary control for rapidly stabilizing the frequency (response time 5 s), secondary control for gradually regulating the frequency to the nominal frequency (response time 5 min) and tertiary control for an economic operation of the power system (response time 15 min). Tertiary control also includes OPF, ED and UC and is usually activated manually. This concept is realized in the Continental Europe power system and has been successful over decades. Similar concepts are utilized all over the world [4]. The concept has, however, limitations. Stability is not guaranteed in the strict sense due to ignoring interactions between primary, secondary and tertiary control. For power systems with large centralized conventional generation units this is not problematic due to large inertias in the generation units which introduce a self-stabilizing effect. For power systems with small decentralized renewable generation units this can be critical due to the lack of large inertias. The decentralization of renewable generation furthermore induces a high complexity. The volatility of renewable generation additionally necessitates very small response times. These issues are difficult to handle with the traditional concept. Novel concepts are strongly required to ensure stability and performance of future power systems.

Smart microgrids (MGs), i.e. clusters of decentralized generation units, storages and loads which are connected over a communication network, are an important concept to address these challenges [5]. Smart MGs have several benefits: (i) Smart MGs can be regarded as a single entity whereby complexity of power system operation and control is decreased substantially. (ii) Smart MGs can be operated virtually independently whereby the dependence on the utility grid can be reduced and the power quality and stability can be improved. (iii) Power is generated and consumed locally whereby transmission losses are reduced. Electric vehicles (EVs) can be utilized in MGs as mobile storages to address volatility [6], [7].

In recent years MGs have been intensively studied in literature and practice. An overview of ongoing practical implementations can be found in the survey paper [5]. The investigations can be divided into two parts, LFC and economic operation of MGs. Economic operation has been considered in [8], [9], [10], [11] while [12], [13], [14] treat LFC of MGs. To the authors' best knowledge a hierarchical control scheme integrating both functionalities has not been considered so far.

This paper presents an energy management system for smart MGs realizing LFC, ED and UC based on hierarchical model predictive control (HiMPC). The energy management system has two levels. On the lower level the frequency is regulated to the nominal frequency on a short time scale (seconds). Short-term variations in renewable generation and load are handled in this way. On the upper level the costs for power generation, starting generators, power exchange with the utility grid as well as power for charging and discharging EVs is minimized on a long time scale (minutes/hours) yielding reference values for the lower level. Long-term variations in renewable generation and load are regarded on the upper level based on predictions. Interactions between the lower level and the upper level are regarded in HiMPC, which is a major improvement over the traditional concept.

The authors are with the Institute of Control Systems, Department of Electrical and Computer Engineering, University of Kaiserslautern, Erwin-Schrödinger-Str. 12, 67663 Kaiserslautern, Germany, E-Mail: berkel|goerges|sliu@eit.uni-kl.de. This work is partly supported by the European Regional Development Fund (ERDF).

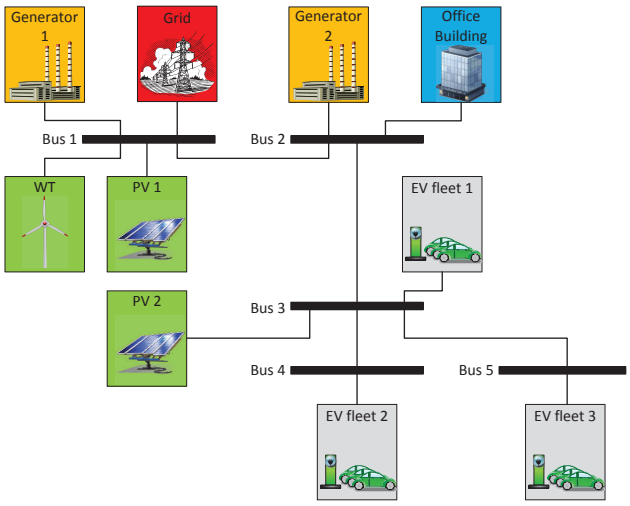

Fig. 1. Topology of the smart microgrid

HiMPC allows covering different time scales, regarding constraints (e.g. power ratings) and predictions (e.g. on renewable generation and load) as well as rejecting disturbances (e.g. due to volatile renewable generation) with guaranteed stability and performance utilizing a systematic model- and optimization-based design. This makes HiMPC very appealing for an energy management in smart MGs.

During the last years HiMPC has received considerable attention [15], [16]. Applications to power systems have been considered only very recently. In [17] a conceptual framework for HiMPC in large-scale power systems has been presented. In [18] an energy management system for smart grids with EVs realizing LFC and ED based on HiMPC has been proposed. This paper extends the concept in [18] in three directions: (i) Besides LFC and ED also UC is covered. To this end a HiMPC based on a mixed-integer linear program (MILP) which can be solved efficiently using standard solvers is developed. This is an important contribution of the paper. (ii) EVs are handled individually instead of aggregately which provides additional degrees of freedom in the optimization. (iii) The model structure of the smart microgrid is exploited for HiMPC.

Throughout the paper, the energy management is evaluated for the smart MG of a company (topology in Fig. 1) with two conventional generation units (e.g. combined heat and power units), two photovoltaic (PV) generation units, a wind turbine (WT), an office building (load) and 150 EVs. The MG is furthermore coupled to the utility grid via a tie line.

The paper is organized as follows: Modeling of the smart MG, precisely the conventional generation units, tie-line power, EVs, load and renewable generation units, is addressed in Section II. HiMPC is presented in Section III. First, the HiMPC structure is outlined. Then, the upper-level and lower-level controllers are detailed. Simulation results are provided in Section IV. Finally, conclusions and remarks on future work are given in Section V.

Throughout the paper, scalars are denoted by non-bold letters, matrices and vectors by bold letters. Furthermore, all powers injected into the grid are positive while powers drawn from the grid are negative.

II. Modeling

First each component of the MG is modeled separately. Then the individual models are combined to an overall model describing the MG.

A. Conventional Generation

The frequency deviation in the MG is characterized by the linear swing equation [19]

$$\Delta \dot{f} = A_{\mathrm{G}} \Delta f + B_{\mathrm{G}} \left(p_{\mathrm{m}} - p_{\mathrm{load}} \right). \tag{1}$$

where $\Delta f = f - f_0$ is the deviation of the actual frequency f from the nominal frequency $f_0 = 50\,\mathrm{Hz}$, p_{m} is the mechanical power of the conventional generators and p_{load} is the electrical power drawn by the electrical loads. The coefficients A_{G} and B_{G} depend on the grid topology and the generators connected to the network. For a detailed description see [19]. Note that (1) describes a condensed model of the MG. Power flow and losses are not considered in the model. For ensuring frequency stability the generated power p_{m} obviously has to be balanced with the load power p_{load}. Moreover, there is a self-stabilizing effect due to the energy stored in the inertia of the generators. Noteworthy, A_{G} and B_{G} depend on the generators connected to the grid, i.e. if generators are switched on/off, then A_{G} and B_{G} can change. This is important when UC is considered.

B. Tie-Line Power

The MG is connected to the utility grid via a tie-line. The power flow p_{T} from the utility grid into the MG can be described by the tie-line power [19]

$$\dot{p}_{\mathrm{T}} = -2\pi \frac{U_{\mathrm{T}} U_{\mathrm{MG}}}{X_{\mathrm{T}}} \Delta f = \hat{p}_{\mathrm{T}} \Delta f. \tag{2}$$

U_{T} is the voltage of the utility grid, U_{MG} is the voltage of the MG and X_{T} is the reactance of the tie-line connecting the utility grid with the MG.

C. Electric Vehicles

A major requirement for grid integration of EVs is that the mobility of the driver is not affected. Controlled charging is necessary to ensure that sufficient energy is stored in the battery when the EV is departing from the grid. Thus, a model describing the energy $e_{\mathrm{EV},i}$ stored in the battery of each EV i is required:

$$\dot{e}_{\mathrm{EV},i} = -\eta_{\mathrm{EV,C}} p^{+}_{\mathrm{EV},i} - \eta_{\mathrm{EV,D}} p^{-}_{\mathrm{EV},i} - p_{\mathrm{drive},i}. \tag{3}$$

Here, the power $p^{\min}_{\mathrm{EV},i} \leq p^{+}_{\mathrm{EV},i} \leq 0$ is the charging power. The power $0 \leq p^{-}_{\mathrm{EV},i} \leq p^{\max}_{\mathrm{EV},i}$ is the discharging power. $p_{\mathrm{drive},i}$ is the power consumption during driving. Furthermore, $\eta_{\mathrm{EV,C}} < 1$ and $\eta_{\mathrm{EV,D}} > 1$ are efficiency factors for charging and discharging the battery, respectively. The energy is subject to physical limitations. The maximum energy which can be stored in the battery is denoted by

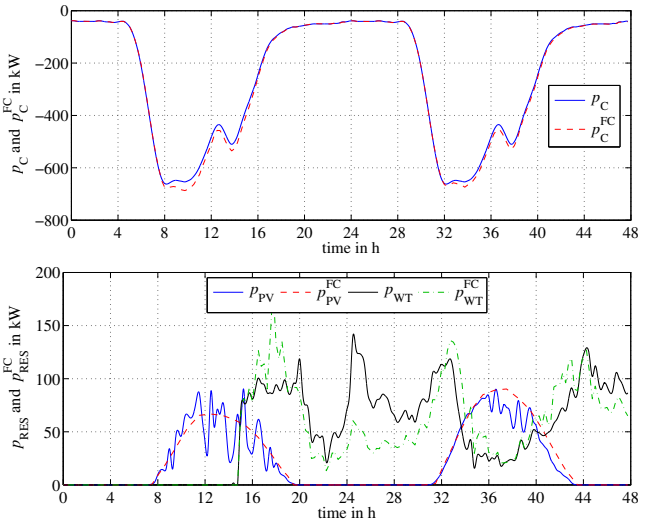

Fig. 2. Load and renewable generation

$e_{\mathrm{EV},i}^{\max}$. The minimum is $e_{\mathrm{EV},i}^{\min}$ which is assumed as 20 % of $e_{\mathrm{EV},i}^{\max}$ to extend the lifetime of the battery. It is furthermore assumed that all EVs are connected to a standard socket with charging/discharging power $\mp$ 3.6 kW. EVs are mobile storages, i.e. EVs can disconnect from the grid and are not available for an energy management in this time. is introduced. The EVs cannot be (dis)charged while driving and vice versa. This can be expressed as

$$\begin{aligned} &\text{EV } i \text{ is disconnected at time } t \Leftrightarrow p_{\mathrm{EV},i}^{+} = p_{\mathrm{EV},i}^{-} = 0 \\ &\text{EV } i \text{ is connected at time } t \Leftrightarrow p_{\mathrm{drive},i} = 0. \end{aligned} \tag{4}$$

D. Load and Renewable Generation

Next the impact of the office building and renewable generation is discussed. The power curve of the office building p_{C} is shown in Fig. 2. Since in this paper demand side-management is not considered, p_{C} cannot be controlled by the energy management. The data corresponds to the standard load profile G1 (industry, weekdays, 8–18 h, scaled) used by German utilities[1]. The power which is fed-in by the photovoltaic generation units is denoted as p_{PV}, the power from the wind turbine as p_{WT}. The power curves for the renewable generation units over two days can be seen in Fig. 2. Similar to the load it is assumed that the infeed from renewable generation units cannot be controlled. Therefore, both the load and the renewable generation units are considered as disturbances $p_{\mathrm{D},i}$ with $i = 1, \ldots, N_{\mathrm{D}}$ and $N_{\mathrm{D}} = 4$. In the HiMPC scheme forecasts of the disturbances are integrated. The forecasts usually do not coincide with the actual values. The data used for the forecast are shown in Fig. 2. These are denoted by $(\cdot)^{\mathrm{FC}}$.

E. Complete MG Model

The models introduced above are combined to two coupled models, one for the MG and one for the EVs. The model of the MG comprises the dynamics of the MG, i.e. the frequency deviation Δf and the tie-line power p_{T}:

$$\begin{aligned} \underbrace{\begin{bmatrix} \Delta \dot{f} \\ \dot{p}_{\mathrm{T}} \end{bmatrix}}_{\dot{\boldsymbol{x}}_{\mathrm{MG}_1}} &= \underbrace{\begin{bmatrix} A_{\mathrm{G}} & B_{\mathrm{G}} \\ \hat{p}_{\mathrm{T}} & 0 \end{bmatrix}}_{\boldsymbol{A}_{\mathrm{MG}_{11}}} \underbrace{\begin{bmatrix} \Delta f \\ p_{\mathrm{T}} \end{bmatrix}}_{\boldsymbol{x}_{\mathrm{MG}_1}} + \underbrace{\begin{bmatrix} B_{\mathrm{G}} & B_{\mathrm{G}} \\ 0 & 0 \\ 0 & 0 \end{bmatrix}}_{\boldsymbol{B}_{\mathrm{MG_{u,11}}}} \underbrace{\begin{bmatrix} p_{\mathrm{G},1} \\ p_{\mathrm{G},2} \end{bmatrix}}_{\boldsymbol{u}_{\mathrm{MG}_1}} \\ &+ \underbrace{\begin{bmatrix} B_{\mathrm{G}} & \cdots & B_{\mathrm{G}} \\ 0 & \cdots & 0 \end{bmatrix}}_{\boldsymbol{B}_{\mathrm{MG_{u,12}}}} \underbrace{\begin{bmatrix} p_{\mathrm{EV},1}^{+} \\ \vdots \\ p_{\mathrm{EV},\mathrm{N_{EV}}}^{-} \end{bmatrix}}_{\boldsymbol{u}_{\mathrm{MG}_2}} \\ &+ \underbrace{\begin{bmatrix} B_{\mathrm{G}} & B_{\mathrm{G}} & B_{\mathrm{G}} \\ 0 & 0 & 0 \end{bmatrix}}_{\boldsymbol{B}_{\mathrm{MG_{d,11}}}} \underbrace{\begin{bmatrix} p_{\mathrm{PV}} \\ p_{\mathrm{WT}} \\ p_{\mathrm{C}} \end{bmatrix}}_{\boldsymbol{d}_{\mathrm{MG}_1}} \end{aligned} \tag{5}$$

The EV model describes the dynamics of the energies $e_{\mathrm{EV},i}$:

$$\begin{aligned} \underbrace{\begin{bmatrix} \dot{e}_{\mathrm{EV},1} \\ \vdots \\ \dot{e}_{\mathrm{EV},\mathrm{N_{EV}}} \end{bmatrix}}_{\dot{\boldsymbol{x}}_{\mathrm{MG}_2}} &= - \underbrace{\begin{bmatrix} \eta_{\mathrm{EV,C}} & \eta_{\mathrm{EV,D}} & 0 & 0 \\ 0 & \ddots & \ddots & 0 \\ 0 & 0 & \eta_{\mathrm{EV,C}} & \eta_{\mathrm{EV,D}} \end{bmatrix}}_{\boldsymbol{B}_{\mathrm{MG_{u,22}}}} \underbrace{\begin{bmatrix} p_{\mathrm{EV},1}^{+} \\ \vdots \\ p_{\mathrm{EV},\mathrm{N_{EV}}}^{-} \end{bmatrix}}_{\boldsymbol{u}_{\mathrm{MG}_2}} \\ &- \underbrace{\begin{bmatrix} 1 & 0 & 0 \\ 0 & \ddots & 0 \\ 0 & 0 & 1 \end{bmatrix}}_{\boldsymbol{B}_{\mathrm{MG_{d,22}}}} \underbrace{\begin{bmatrix} p_{\mathrm{drive},1} \\ \vdots \\ p_{\mathrm{drive},\mathrm{N_{EV}}} \end{bmatrix}}_{\boldsymbol{d}_{\mathrm{MG}_2}} \end{aligned} \tag{6}$$

N_{EV} is the number of EVs. The dynamics of the MG and the EVs are almost decoupled. The only connection between them is $\boldsymbol{u}_{\mathrm{MG}_2}$ which is the (dis)charging power of the EVs. This special structure can be exploited in the controller design.

III. Hierarchical Control Structure

A hierarchical control structure generally consists of several levels where each level works with a specific sampling time. Usually, the levels are ordered according their sampling time and the level with the larger sampling time computes references for the level with smaller sampling time. Since the control scheme works in discrete-time in the following discrete-time models are considered.

The control structure applied to the MG is shown in Fig. 3. The controller is structured hierarchically and comprises two levels. The upper level calculates economically optimal reference values $\boldsymbol{u}_{\mathrm{MG}_1}^{\mathrm{ref}}$ and $\boldsymbol{x}_{\mathrm{MG}_1}^{\mathrm{ref}}$ for the lower level and controls the energy of the EV batteries using (6). For the economic optimization additional models are developed in Section III-A. The lower level controls the frequency and the tie-line power in the MG using (5). The energies of the EV batteries are not considered on the lower level. Furthermore, the upper level calculates the input variables $\boldsymbol{u}_{\mathrm{MG}_2}$, i.e. it calculates the (dis)charging power of the EV batteries. Of course the input variables also affect $\boldsymbol{x}_{\mathrm{MG}_1}$ but since the lower level works with a smaller sampling time than the upper level, the input variables $\boldsymbol{u}_{\mathrm{MG}_2}$ can be regarded as

[1] http://www.uez.de/Standardisierte_Lastprofile.html, values for June 20, 2011

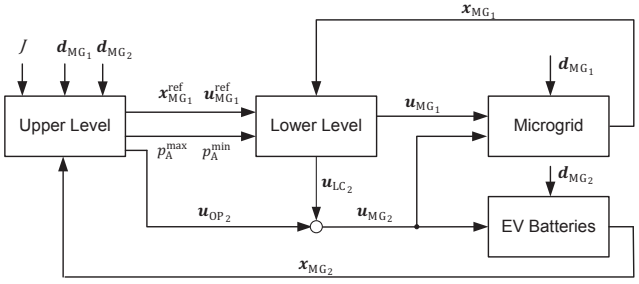

Fig. 3. Hierarchical control structure

known slowly varying disturbances from the lower level point of view.

To use the EV batteries also for power balancing on the time scale of the lower level, $\boldsymbol{u}_{\mathrm{MG}_2}$ is split up into parts:

$$\boldsymbol{u}_{\mathrm{LC}_2} = \begin{bmatrix} \Delta p^{+}_{\mathrm{EV},1} \\ \Delta p^{-}_{\mathrm{EV},1} \\ \vdots \\ \Delta p^{-}_{\mathrm{EV},\mathrm{N_{EV}}} \end{bmatrix}, \boldsymbol{u}_{\mathrm{OP}_2} = \begin{bmatrix} p^{+}_{\mathrm{EV},1} \\ p^{-}_{\mathrm{EV},1} \\ \vdots \\ p^{-}_{\mathrm{EV},\mathrm{N_{EV}}} \end{bmatrix}. \quad (7)$$

$\boldsymbol{u}_{\mathrm{OP}_2}$ is the power calculated by the upper level and $\boldsymbol{u}_{\mathrm{LC}_2}$ is the power calculated by the lower level.

$\Delta p^{+}_{\mathrm{EV},i}$ and $\Delta p^{-}_{\mathrm{EV},i}$ are additional power outputs for each EV which are calculated by the lower-level controller. Thus, the lower level has the possibility to use the EV batteries for frequency regulation on a short time scale which makes the frequency control algorithm more dynamic.

Of course $\boldsymbol{u}_{\mathrm{LC}_2}$ has to be integrated into the state-space model for the lower-level controller design. An aggregation is used here. Since the frequency controller has to reject disturbances on a short time scale, it is executed with smaller sampling time than the upper-level controller. Thus, the control problem formulation has to be simpler to ensure real-time control. Thus, the lower-level controller works with an aggregated model of the EVs, i.e. in the controller model a single power p_{A} which is the sum of all powers is considered instead of the power of every EV. The aggregation does not guarantee to be optimal. However, since power dispatch is dominated by the optimization at the upper level, this can be neglected in the lower level.

The upper level calculates optimal inputs $\boldsymbol{u}_{\mathrm{OP}_2}$ for EVs for the next time step based on a prediction of the load and then renewable in-feed with a larger sampling time than the one of the lower-level controller. Without modification, it is possible that the lower-level controller can change these calculated values completely through manipulating $\boldsymbol{u}_{\mathrm{LC}_2}$. To restrict the influence of the lower-level controller on the EV batteries, the upper-level controller provides the lower-level controller with bounds on p_{A}. The bounds $p_{\mathrm{A}}^{\min}$ and $p_{\mathrm{A}}^{\max}$ ensure that the influence of the lower-level controller on the EV batteries is held very small so that the optimal trajectories computed by the upper level are not jeopardized. Moreover, the bounds on maximum/minimum power and energy of the EVs are not violated.

An important issue in HiMPC is stability. Stability is not studied formally in this paper. However, some principal considerations on stability are provided in the following. Due to the larger sampling time of the upper level compared to the lower level, the lower-level controller can destabilize the upper-level controller. Nevertheless, with the introduction of the bounds on the aggregated power p_{A} and the recomputation of these bounds each sampling instant of the upper level, the lower-level controller cannot bring the control scheme to infeasibility. Nor can the lower-level controller destabilize the upper-level controller since the influence of the lower-level controller on the batteries is limited by $p_{\mathrm{A}}^{\min}$ and $p_{\mathrm{A}}^{\max}$. Even in the worst case when the lower-level controller would hit the constraints of the EVs, the bounds on the aggregated power are set to zero to render destabilization impossible.

Note that similar stability criteria have been presented in [20]. Further stability criteria for HiMPC have been developed in [21] based on robust control theory.

A. Upper-Level Controller

The main goal of the upper-level controller is minimizing the operational cost of the MG. This requires a cost function that comprises the cost for storing and generating energy. The optimization problem is defined as

$$\min \sum_{k=0}^{N_{\mathrm{u}}-1} \left(\sum_{i=1}^{N_{\mathrm{G}}} \left[J_{\mathrm{G},i}(k) + J^{\mathrm{A}}_{\mathrm{S},i}(k) \right] + J_{\mathrm{T}}(k) + \sum_{i=1}^{N_{\mathrm{EV}}} J_{\mathrm{EV},i}(k) \right), \quad (8)$$

where $N_{\mathrm{G}} = 2$ is the number of generators and N_{u} is the prediction horizon of the upper-level controller. $J_{\mathrm{G},i}(k)$ is the cost for output power from the generators, $J^{\mathrm{A}}_{\mathrm{S},i}(k)$ is the approximated cost for starting the generators, $J_{\mathrm{T}}(k)$ is the cost for buying/selling power from/to the utility grid and $J_{\mathrm{EV},i}(k)$ is the cost for (dis)charging the EVs. The costs for the load and the renewable generation are assumed to be zero since they cannot be influenced. The optimization variables are $p_{G,i}(k), \delta_{G,i}(k), p^{+/-}_{EV,i}(k), p^{+/-}_{T}(k)$. These variables and the constraints are detailed in the following sections. Note that in (8) $k+h$ with k being the actual sampling instant and h the time index is abbreviated by k for brevity.

1) Conventional Generation: Since the demand for power varies significantly over the day, generators can be operated more efficiently when they can be switched on/off. This requires the introduction of the binary variables $\delta_{\mathrm{G},i}(k)$:

$\delta_{\mathrm{G},i}(k) = 0 \Leftrightarrow$ generator i is switched off at time instant k

$\delta_{\mathrm{G},i}(k) = 1 \Leftrightarrow$ generator i is switched on at time instant k

The optimization problem can then be formulated as an MILP. The cost of a generator $J_{\mathrm{G},i}(k)$ is usually given by a quadratic function [3, Ch. 3]:

$$J_{\mathrm{G},i}(k) = a_i \delta_{\mathrm{G},i}(k) p_{\mathrm{G},i}(k)^2 + b_i \delta_{\mathrm{G},i}(k) p_{\mathrm{G},i}(k) + c_i. \quad (9)$$

The cost comprises fuel and maintenance costs of the generators. For $a_i > 0$, $J_{\mathrm{G},i}(k)$ is a strict convex function. Thus, the cost function can easily be approximated by piecewise affine (PWA) functions. Approximation methods can e.g. be

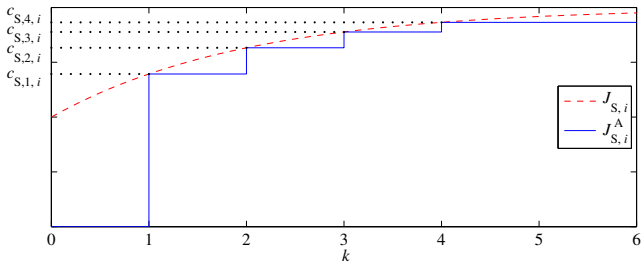

Fig. 4. Start-up Cost

found in [22, Sec. 7.3]. Using a PWA function the cost can be integrated in an MILP.

When a generator is switched off, the steam inside the turbine starts to cool down. When it is restarted again, the steam has to be reheated. The starting cost $J_{\mathrm{S},i}$ and can be described by an exponential function [3, Ch. 5]:

$$J_{\mathrm{S,i}}(t) = c_{\mathrm{S,cold},i}\left(1 - e^{-t/t_{\mathrm{c}}}\right) + c_{\mathrm{S,fix},i} \tag{10}$$

where t is the time, $c_{\mathrm{S,cold},i}$ is the cold start cost, $c_{\mathrm{S,fix},i}$ are fixed start-up costs and t_{c} is the time constant of the cooling process. For integration of $J_{\mathrm{S},i}$ in an MILP a stair-wise approximation $J^{\mathrm{A}}_{\mathrm{S},i}$ is used [23]:

$$\begin{aligned} J^{\mathrm{A}}_{\mathrm{S},i}(k) &\geq c_{\mathrm{S},l,i}\left(\delta_{\mathrm{G},i}(k) - \sum_{j=1}^{l}\delta_{\mathrm{G},i}(k-j)\right) \\ J^{\mathrm{A}}_{\mathrm{S},i}(k) &\geq 0, k \in \{1,...,N_{\mathrm{u}}\}, l \in \{1,...,N_{\mathrm{S}}\}. \end{aligned} \tag{11}$$

The original and approximated costs are depicted in Fig. 4. The stair-wise costs $c_{\mathrm{S},l,i} > 0$ for starting the unit at each sampling instant are depicted. l is the index for each cost and is of the set $\{1,...,N_{\mathrm{S}}\}$ where N_{S} is the number of stairs in the approximation.

Furthermore, the lifetime of a generator can be shortened when the generators are frequently switched on/off. Therefore, minimum downtime and minimum uptime are defined. The minimum uptime/downtime constraint ensures that the generator stays online/offline when it is started/shut down. The minimum downtime constraints can be expressed as [24]

$$\begin{aligned} &\delta_{\mathrm{G},i}(k-1) - \delta_{\mathrm{G},i}(k) \leq 1 - \delta_{\mathrm{G},i}(j) \qquad (12)\\ &\forall k = 1,...,N_{\mathrm{u}},\ j = k+1,...,\min\{k+\tau_{\mathrm{dt},i}-1, N_{\mathrm{u}}\} \\ &\delta_{\mathrm{G},i}(k+j) = 0 \qquad (13)\\ &\forall j = 1,...,\max\{k_{\mathrm{off},i} - (k-\tau_{\mathrm{dt},i}), 0\} \end{aligned}$$

where $\tau_{\mathrm{dt},i}$ is the minimum downtime of generator i and $k_{\mathrm{off},i}$ is the sampling instant at which unit i has been shut down. Equation (12) ensures that generator i meets the minimum down time in the future while (13) ensures that if a generator is within its minimum downtime at sampling instant $k = 0$ it stay offline until expiry. The minimum uptime is analogously defined as

$$\begin{aligned} &-\delta_{\mathrm{G},i}(k-1) + \delta_{\mathrm{G},i}(k) \leq \delta_{\mathrm{G},i}(j) \qquad (14)\\ &\forall k = 1,...,N_{\mathrm{u}},\ j = k+1,...,\min\{k+\tau_{\mathrm{ut},i}-1, N_{\mathrm{u}}\} \\ &\delta_{\mathrm{G},i}(k+j) = 1 \qquad (15)\\ &\forall j = 1,...,\max\{k_{\mathrm{on},i} - (k-\tau_{\mathrm{ut},i}), 0\}. \end{aligned}$$

where $\tau_{\mathrm{ut},i}$ is the minimum uptime of generator i and $k_{\mathrm{on},i}$ is the sampling instant at which unit i has been switched on.

The output power of the generators cannot be changed arbitrarily. Therefore, ramp constraints for each generator i are added to the MILP [23]:

$$\begin{aligned} &-\delta_{\mathrm{G},i}(k-1)\,p_{\mathrm{G},i}(k-1) + \delta_{\mathrm{G},i}(k)\,p_{\mathrm{G},i}(k) \\ &\geq -\Delta p^{\min}_{\mathrm{G},i}\delta_{\mathrm{G},i}(k-1) - p^{\max}_{\mathrm{G},i}\left[1 - \delta_{\mathrm{G},i}(k)\right], \\ &\delta_{\mathrm{G},i}(k-1)\,p_{\mathrm{G},i}(k-1) - \delta_{\mathrm{G},i}(k)\,p_{\mathrm{G},i}(k) \\ &\geq -\Delta p^{\max}_{\mathrm{G},i}\delta_{\mathrm{G},i}(k) + p^{\max}_{\mathrm{G},i}\left[\delta_{\mathrm{G},i}(k) - 1\right]. \end{aligned} \tag{16}$$

Furthermore, at least one generation unit has to be switched on to get the stabilizing effect of the rotating masses (cf. Section II-A). This can be ensured by the logical constraint

$$\sum_{i=1}^{N_{\mathrm{G}}}\delta_{\mathrm{G},i}(k) \geq 1. \tag{17}$$

As already mentioned scheduling leads to time-varying parameters A_{G} and B_{G} in (1). Since at least one of the two generators has to be switched on, there are three possible values for A_{G} and B_{G}.

2) Tie-Line Power: The costs for buying/selling power from/to the grid are defined by

$$J_{\mathrm{T}}(k) = c_{\mathrm{T,B}}p^{+}_{\mathrm{T}}(k) + c_{\mathrm{T,S}}p^{-}_{\mathrm{T}}(k) \tag{18}$$

where $c_{\mathrm{T,B}}$ is the marginal cost for buying power from the grid and $c_{\mathrm{T,S}}$ is the marginal revenue for selling power to the grid. Similar as the output power of the EVs, the tie-line power p_{T} is split in two powers $0 \leq p^{+}_{\mathrm{T}} \leq p^{\max}_{\mathrm{T}}$ and $p^{\min}_{\mathrm{T}} \leq p^{-}_{\mathrm{T}} \leq 0$ in the computation of the upper level to allow different costs for buying and selling power.

3) Electric Vehicles: The cost function for EV i is

$$J_{\mathrm{EV},i}(k) = c_{\mathrm{EV,B},i}p^{+}_{\mathrm{EV},i}(k) + c_{\mathrm{EV,S},i}p^{-}_{\mathrm{EV},i}(k) \tag{19}$$

where $c_{\mathrm{EV,B},i} < 0$ and $c_{\mathrm{EV,S},i} > 0$ are the marginal cost and revenue for charging and discharging the battery. Since the optimization operates in discrete-time, (3) is discretized with sampling time T_{u}. The usage of EVs for frequency regulation must not restrict the mobility of the owners, i.e. the vehicles must be sufficiently charged at departure. To achieve this the inequality constraint

$$e_{\mathrm{EV},i}\left(t^{\mathrm{p}}_{\mathrm{dep},i} - \Delta t_{\mathrm{dep},i}\right) \geq e_{\mathrm{d},i}\ \text{, for } i = 1,...N_{\mathrm{EV}}. \tag{20}$$

for the planned departure time $t^{\mathrm{p}}_{\mathrm{dep},i}$ is added where $e_{\mathrm{d},i}$ is the minimum desired energy stored in the EV battery at departure and $\Delta t_{\mathrm{dep},i}$ is the maximum deviation from the planned departure time. $e_{\mathrm{d},i}$ can be calculated before departure by

$$e_{\mathrm{d},i} = \left(d^{\mathrm{p}}_{i} + \Delta d_i\right) l_{\mathrm{EV},i} \tag{21}$$

where d^{p}_{i} is the planned driving distance, Δd_i denotes the maximum deviation from the planned driving distance and $l_{\mathrm{EV},i}$ is the average power consumption. While driving the EVs are not connected to the MG and consequently the actual

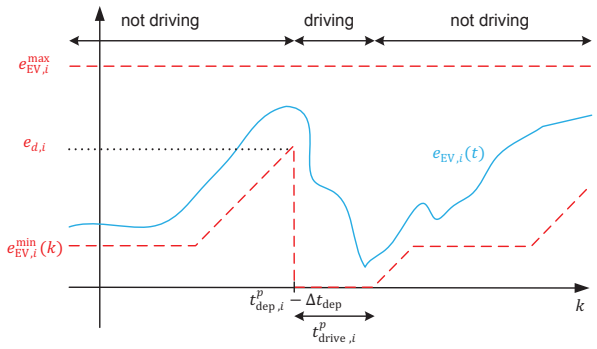

Fig. 5. Constraints on the battery energy of EV i

energy $e_{\mathrm{EV_{act}},\mathrm{i}}(k)$ of the EV battery is not available for the energy management system. This can be regarded by

$$e_{\mathrm{EV},\mathrm{i}}(k) = \begin{cases} e_{\mathrm{EV_{act}},\mathrm{i}}(k) & \text{if EV } i \text{ connected at } k \\ 0 & \text{if EV } i \text{ connected at } k. \end{cases} \quad (22)$$

Also the battery power is zero in this time, i.e.

$$p^{+}_{\mathrm{EV},\mathrm{i}}(k) = p^{-}_{\mathrm{EV},\mathrm{i}}(k) = 0 \quad \text{if EV } i \text{ disconnected at } k \quad (23)$$

While driving the upper level has to predict the energy $e_{\mathrm{EV},\mathrm{i}}(k)$ of the EVs. One possibility to do this is to compute the average battery power

$$p_{\mathrm{drive},i}(k) = \frac{(d^{\mathrm{p}}_i + \Delta d_i) \cdot l_{\mathrm{EV},i}}{t^{\mathrm{p}}_{\mathrm{drive},i}} \quad (24)$$

where $t^{\mathrm{p}}_{\mathrm{drive},i}$ is the planned driving time. The actual power consumption is usually not constant but this is not essential for the upper level.

The energy curve and its constraints can be seen in Fig. 5. One can see that the lower bound on the energy consumption rises linearly before departure time. Loosely speaking, additional constraints can be helpful to speed up the solution time in an MILP. In the simulation, it has been observed that the time-varying bounds speed up the solution time although they are not necessary for ensuring fully charged EVs at departure time.

4) Power Balance: As mentioned in Section II-A it is essential that the sum of all powers is zero, i.e.

$$0 = \sum_{i=1}^{N_{\mathrm{G}}} p_{\mathrm{G},i}(k)\,\delta_{\mathrm{G},i}(k) + \sum_{i=1}^{N_{\mathrm{EV}}} \left(p^{+}_{\mathrm{EV},i}(k) + p^{-}_{\mathrm{EV},i}(k)\right) + \sum_{i=1}^{N_{\mathrm{D}}} p_{\mathrm{D},i}(k) + p^{+}_{\mathrm{T}}(k) + p^{-}_{\mathrm{T}}(k)\ \forall k = 0, ..., N_{\mathrm{u}} - 1.$$

B. Lower-Level Controller

The purpose of the lower-level controller is to control the frequency of the MG. For the model of the controller the MG dynamics are augmented with the aggregated power p_{A} as an additional input for balancing the frequency on a short time scale. This yields the following continuous-time model

$$\dot{\boldsymbol{x}}_{\mathrm{LC}} = \boldsymbol{A}_{\mathrm{LC_c}}\,\boldsymbol{x}_{\mathrm{LC}} + \boldsymbol{B}_{\mathrm{LC_{u,c}}}\boldsymbol{u}_{\mathrm{LC_1}} + \boldsymbol{B}_{\mathrm{LC_{d,c}}}\boldsymbol{d}_{\mathrm{LC}} \quad (25)$$

EV type	l_{EV}	$e^{\max}_{\mathrm{EV}}$
1	13.5 KWh	16 $^{\mathrm{KWh}}/_{100\mathrm{km}}$
2	15.1 KWh	17.6 $^{\mathrm{KWh}}/_{100\mathrm{km}}$
3	18 KWh	24 $^{\mathrm{KWh}}/_{100\mathrm{km}}$
4	21 KWh	22 $^{\mathrm{KWh}}/_{100\mathrm{km}}$
5	21 KWh	24 $^{\mathrm{KWh}}/_{100\mathrm{km}}$

TABLE I
EV PARAMETERS

where

$$\boldsymbol{u}_{\mathrm{LC_1}} = \begin{bmatrix} \boldsymbol{u}_{\mathrm{MG_1}} \\ p_{\mathrm{A}} \end{bmatrix}, \boldsymbol{B}_{\mathrm{LC_{u,c}}} = \begin{bmatrix} B_{\mathrm{G}} & B_{\mathrm{G}} & B_{\mathrm{G}} \\ 0 & 0 & 0 \end{bmatrix} \quad (26)$$

and $\boldsymbol{x}_{\mathrm{LC}} = \boldsymbol{x}_{\mathrm{MG_1}}$, $\boldsymbol{A}_{\mathrm{LC_c}} = \boldsymbol{A}_{\mathrm{MG_{11}}}$, $\boldsymbol{B}_{LC_{d,c}} = \boldsymbol{B}_{\mathrm{MG_{d,11}}}$, $\boldsymbol{d}_{\mathrm{LC}} = \boldsymbol{d}_{\mathrm{MG_1}}$.

A standard linear MPC controller is applied:

$$\begin{aligned} \min_{\boldsymbol{u}_{\mathrm{LC_1}}(k)} \ & |\boldsymbol{P}\,\tilde{\boldsymbol{x}}_{\mathrm{LC}}(N)|_2 + \sum_{k=0}^{N_{\mathrm{l}}-1} |\boldsymbol{Q}\,\tilde{\boldsymbol{x}}_{\mathrm{LC}}(k)|_2 + |\boldsymbol{R}\,\tilde{\boldsymbol{u}}_{\mathrm{LC_1}}(k)|_2 \\ \text{s.t.} \quad & \boldsymbol{x}_{\mathrm{LC}}(k+1) = \boldsymbol{A}_{\mathrm{LC_d}}\boldsymbol{x}_{\mathrm{LC}}(k) + \boldsymbol{B}_{\mathrm{LC_{u,d}}}\boldsymbol{u}_{\mathrm{LC_1}}(k), \\ & \quad + \boldsymbol{B}_{\mathrm{LC_{d,d}}}\boldsymbol{d}_{\mathrm{LC}}(k) \\ & \tilde{\boldsymbol{x}}_{\mathrm{LC}}(k) = \boldsymbol{x}_{\mathrm{LC}}(k) - \boldsymbol{x}^{\mathrm{ref}}_{\mathrm{LC}}(k), \\ & \tilde{\boldsymbol{u}}_{\mathrm{LC_1}}(k) = \boldsymbol{u}_{\mathrm{LC_1}}(k) - \boldsymbol{u}^{\mathrm{ref}}_{\mathrm{LC_1}}(k), \\ & \boldsymbol{x}^{\min}_{\mathrm{LC}} \le \boldsymbol{x}_{\mathrm{LC}}(k) \le \boldsymbol{x}^{\max}_{\mathrm{LC}}, \\ & \boldsymbol{u}^{\min}_{\mathrm{LC_1}}(k) \le \boldsymbol{u}_{\mathrm{LC_1}}(k) \le \boldsymbol{u}^{\max}_{\mathrm{LC_1}}(k), \\ & -\Delta\boldsymbol{u}^{\min}_{\mathrm{LC_1}} \le \Delta\boldsymbol{u}_{\mathrm{LC_1}}(k) \le \Delta\boldsymbol{u}^{\max}_{\mathrm{LC_1}}, \\ & \Delta\boldsymbol{u}_{\mathrm{LC_1}}(k) = \boldsymbol{u}_{\mathrm{LC_1}}(k) - \boldsymbol{u}_{\mathrm{LC_1}}(k-1). \end{aligned}$$

The system matrices $\boldsymbol{A}_{\mathrm{LC_d}}$, $\boldsymbol{B}_{\mathrm{LC_{u,d}}}$ and $\boldsymbol{B}_{\mathrm{LC_{d,d}}}$ are the system matrices of the discrete-time model to (25). The sampling time is $T_l = 0.5\,\mathrm{s}$. $\boldsymbol{Q}$ and $\boldsymbol{R}$ are weighting matrices to penalize the deviation of states and inputs from their references. $\boldsymbol{P}$ penalizes deviations of the final state from its reference. N_{l} is the prediction horizon. The bounds on the generators in the lower level are softened compared to the upper level in order to provide the lower-level controller with more flexibility in frequency balancing. Note that the bounds on the input $\boldsymbol{u}^{\min}_{\mathrm{LC_1}}(k)$ and $\boldsymbol{u}^{\max}_{\mathrm{LC_1}}(k)$ are time-varying for two reasons. First, the bounds on the aggregated power p_{A} are time-varying (cf. Section III). Second, scheduling of the generators is only possible by the upper-level controller. To prevent the lower-level controller from scheduling, the bounds on generator i are set to $p^{\max}_{\mathrm{G},i} = p^{\min}_{\mathrm{G},i} = 0$ when it is switched off. Moreover, the system matrices $\boldsymbol{A}_{\mathrm{LC_d}}$, $\boldsymbol{B}_{\mathrm{LC_{u,d}}}$ and $\boldsymbol{B}_{\mathrm{LC_{d,d}}}$ are time-varying as the scheduling of the generators influences the coefficients A_{G} and B_{G} in (1). The aggregated power p_{A} is distributed on $\boldsymbol{u}_{\mathrm{LC_2}}$ using the relation given by $\boldsymbol{u}_{\mathrm{OP_2}}$. Note that the abbreviation k for $k+h$ is used for brevity again.

IV. Simulation

A. Simulation Setup

Simulations for evaluating the energy management system are performed for the smart MG of a company. There are 150 EVs available which can be used by the employees for business trips. It is assumed that the company has 5 different

kinds of EVs. The parameters of the EVs which are required for the simulation are the maximum capacity of the batteries $e_{\mathrm{EV}}^{\max}$ and the average consumption per $100\,\mathrm{km}$ l_{EV}. These parameters for each EV type are shown in Table I. Note that the simulation model is equivalent to the model used for controller design.

In a realistic scenario, the employees are able to book the EVs over a fleet management system. From the fleet management system $\left(d_i^{\mathrm{p}}, t_{\mathrm{dep},i}^{\mathrm{p}}\right)$ is available to the upper level. For the simulation this data has to be generated. To this end random departure and arrival times with normal distribution (mean value 8 h for departure time, mean value 16 h for arrival time, variance 1 h) are generated. Furthermore, random travel distances with normal distribution (mean value 70 km, variance is 10 km) are generated. The planned and actual times and distances can differ. To model this in the optimization the deviations from planned departure and driving times $\Delta t_{\mathrm{dep},i}$ and $\Delta t_{\mathrm{drive},i}$ as well as the deviations from the planned travel distances $d_{\mathrm{p},i}$ are included. To keep the complexity of the simulation low, it is assumed that the departure time is an integer multiple of the sampling time of the upper-level controller. Random deviations with uniform distribution uniformly are generated. The bounds on the deviation of the distance are $\Delta d_i = \pm 10\,\mathrm{km}$. The bounds on the deviation of the departure time and the arrival time are $\pm 0.25\,\mathrm{h}$. Noteworthy, it is assumed that about 30 EVs do not depart and thus are available for energy management all the time. The remaining parameters are given in Table II. The MG and EV dynamics are simulated over 24h.

Description	Parameter	Value
Number of generators	N_{G}	2
Number of EVs	N_{EV}	150
Number of disturbances	N_{D}	4
Nominal frequency	f_0	50 Hz
Swing-equation parameter	A_{G}	-7.62 | -14.22 | -4.96
Swing-equation parameter	B_{G}	14.29 | 26.68 | $9.30 \cdot 10 - 3\ ^{\mathrm{Hz}}/_{\mathrm{kW}}$
Tie-line power constant	$\hat{p}_{\mathrm{T}}$	$2.5\ ^{\mathrm{MW}}/_{\mathrm{Hz}}$
Max. power generators	$p_{\mathrm{G},1\|2}^{\max}$	400 | 250 kW
Min. power generators	$p_{\mathrm{G},1\|2}^{\min}$	200 | 125 kW
Max. rate power generators	$\Delta p_{\mathrm{G},1\|2}^{\max}$	50 | 40 kW
Min. rate power generators	$\Delta p_{\mathrm{G},1\|2}^{\min}$	-50 | -40 kW
Min. uptime generators	$\tau_{\mathrm{ut},1\|2}$	2 | 1.5 h
Min. downtime generators	$\tau_{\mathrm{dt},1\|2}$	2 | 1.5 h
Time constant start-up cost	$t_{\mathrm{su},1\|2}$	6 | 3 h
Cold start cost generator	$c_{\mathrm{S,cold},1\|2}$	900 | 500 Ct
Fixed cost starting generator	$c_{\mathrm{S,fix},1\|2}$	900 | 500 Ct
No. approximations start-up cost	N_{S}	15
Cost coefficient generators	$a_{1\|2}$	0 | 0 Ct
Cost coefficient generators	$b_{1\|2}$	3.25 | $3.5\ ^{\mathrm{Ct}}/_{\mathrm{kW}}$
Cost coefficient generators	$c_{1\|2}$	$3.25 \cdot 10^{-3}\,^{\mathrm{Ct}}/_{\mathrm{kW}^2}$ | $3.5 \cdot 10^{-3}\,^{\mathrm{Ct}}/_{\mathrm{kW}^2}$
Max. charging/discharging power	$p_{\mathrm{EV},i}^{\max\|\min}$	$\pm$ 3.6 kW
Efficiency factors of EVs	$\eta_{\mathrm{EV,C\|D}}$	0.98 | 1.02
Max./min. tie-line power	$p_{\mathrm{T}}^{\max\|\min}$	$\pm$250 kW
Marginal cost tie-line power	$c_{\mathrm{T,B\|S}}$	6.25 | $2.5\ ^{\mathrm{Ct}}/_{\mathrm{kW}}$
Marginal cost EV power	$c_{\mathrm{EV,B\|S},i}$	$\mp\ 2.5 \cdot 10^{-4}\ ^{\mathrm{Ct}}/_{\mathrm{kW}}$
Horizon upper/lower level	$N_{\mathrm{u\|l}}$	96 | 20
Sampling time upper/lower level	$T_{\mathrm{u\|l}}$	900 | 0.5 s
Weighting matrix	$\boldsymbol{Q}$	diag(1000, 50)
Weighting matrix	$\boldsymbol{R}$	diag(50, 50, 1)

TABLE II
SYSTEM PARAMETERS

B. Simulation Results

Figure 6a) shows the frequency deviation from the nominal value. One can observe that the frequency deviation increases when the generator 1 is switched off. This is due to the changed inertia. When both generators are connected, the inertia of the rotating masses in the MG is higher which has a stabilizing effect on the frequency. The tie-line power is shown in Fig. 6b). One can observe that when the load power is rising between 5 h and 8 h, power is drawn from the grid as well since the power lack cannot completely be compensated by the EVs. Furthermore, from the figure it can be seen that between 10 h and 15 h when most of the EVs are away the tie-line power is used to balance the power on a short time scale. Furthermore, tie-line power is used in extreme situations, e.g. if the consumption is rising or falling. Without support of the tie-line the frequency deviations are higher. In Fig. 6c) one can see the output power from generator 1. One can observe that the generator respects its bounds. The same is true for generator 2 in Fig. 6d). At about 16 h generator 1 is shut down since the demand for power is low in the evening. The curve of the EV power is depicted in Fig. 6e). One can observe that the generators store energy in the EVs which is used to balance the peak. The EVs are charged in the morning and the energy is used to balance the peak load later about noon. During the working hours the power is very low since most of the EVs have left for their journey. In the evening the EVs are charged again using power from the wind turbine. In Fig. 6f) the aggregated power p_{A} and its time-varying constraints are shown. One can see that the power is used for balancing of power on a short time scale, especially when the load is rising in the morning or decreasing in the evening. In the working hours the constraints are very small since most of the EVs are disconnected and so the possibility to compensate power lacks is low. This matches with the observation that the controller uses the tie-line power in this time. In the evening, most EVs have arrived at the MG again and thus the constraints become softer again. The power curve and the energy of EV 53 is shown in the Figs. 6g) and 6h). One can see that the upper level respects the limitations of the EVs due to mobility. The MILPs are solved with the IBM® ILOG® solver CPLEX® 12.4. All calculations have been performed on a PC with Intel® i7-2640M processor with 2.8 GHz and 8 GB RAM under Windows 7 Home Premium®. The maximum solver time is 192.35 s and the average solver time is 87.18 s with optimality tolerance of $\epsilon = 0.35\%$. Thus the MILP can be solved in real-time with upper-level sampling time $T_{\mathrm{u}} = 900\,\mathrm{s}$.

V. CONCLUSIONS AND FUTURE WORK

Within this paper a hierarchical control scheme with two levels for smart MGs has been studied. In the upper level

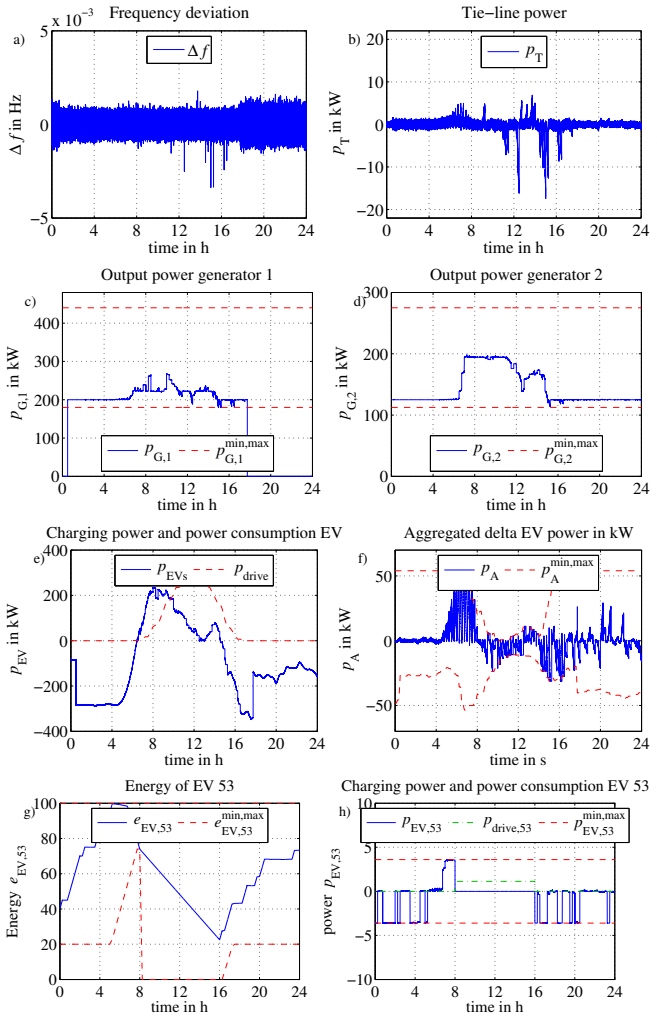

Fig. 6. Simulation Results

an optimization scheme is installed. In the lower level a controller that controls the frequency is used. With the help of MILP scheduling of the generators is possible. EVs have been integrated directly in the optimization scheme without aggregation. The EVs are optimally used for power dispatch and simultaneously the mobility demand of the users is not impaired. Moreover, an integration of EVs can help to improve the power balance and therefore stability of the MG. Furthermore, simulations of the hierarchical structure indicate that the control of the frequency with the proposed control scheme is possible. Future work will focus on incorporating OPF into HiMPC. Particularly, line limits and losses will be regarded. Furthermore, a formal stability proof will be derived. Finally, an islanded operation of the MG will be studied.

REFERENCES

[1] Federal Republic of Germany, Federal Ministry for the Environment, Nature Conservation and Nuclear Safety, "Renewable energy sources in figures," Study, July 2011, http://www.bmu.de/files/english/pdf/application/pdf/broschuere_ee_zahlen_en_bf.pdf.

[2] ——, "National renewable energy action plan in accordance with Directive 2009/28/EC on the promotion of the use of energy from renewable sources," August 2010, http://ec.europa.eu/energy/renewables/transparency_platform/doc/national_renewable_energy_action_plan_germany_en.pdf.

[3] A. J. Wood and B. Wollenberg, *Power Generation, Operation & Control*. New York: John Wiley & Sons, 1984.

[4] Y. G. Rebours, D. S. Kirschen, M. Trotignon, and S. Rossignol, "A survey of frequency and voltage control ancillary services—Part I: Technical features," *IEEE Transactions on Power Systems*, vol. 22, no. 1, pp. 350–357, 2007.

[5] N. Hatziargyriou, H. Asano, R. Iravani, and C. Marnay, "An overview of ongoing research, development, and demonstration projects," *IEEE Power & Energy Magazine*, vol. 5, no. 4, pp. 79–94, 2007.

[6] W. Su, H. Rahimi-Eichi, W. Zeng, and M.-Y. Chow, "A survey on the electrification of transportation in a smart grid environment," *IEEE Transactions on Industrial Informatics*, vol. 8, no. 1, pp. 1–10, 2012.

[7] N. Leemput, J. Van Roy, F. Geth, P. Tant, B. Claessens, and J. Driesen, "Comparative analysis of coordination strategies for electric vehicles," in *Proceedings of the 2011 IEEE PES Innovative Smart Grid Technologies Conference Europe*, 2011.

[8] A. Dimeas and N. Hatziargyriou, "Operation of a multiagent system for microgrid control," *IEEE Transactions on Power Systems*, vol. 20, no. 3, pp. 1447–1455, 2005.

[9] M. López, S. Martín, J. Aguado, and S. de la Torre, "Optimal microgrid operation with electric vehicles," in *Proceedings of the 2011 IEEE PES Innovative Smart Grid Technologies Conference Europe*, 2011, pp. 1–8.

[10] A. Parisio and L. Glielmo, "Energy efficient microgrid management using model predictive control," in *Proceedings of the 50th IEEE Conference on Decision and Control and European Control Conference*, 2011, pp. 5449–5454.

[11] A. Tsikalakis and N. Hatziargyriou, "Centralized control for optimizing microgrids operation," *IEEE Transactions on Energy Conversion*, vol. 23, no. 1, pp. 241 –248, 2008.

[12] F. Katiraei and M. Iravani, "Power management strategies for a microgrid with multiple distributed generation units," *IEEE Transactions on Power Systems*, vol. 21, no. 4, pp. 1821–1831, 2006.

[13] J. P. Lópes, C. Moreira, and A. Madureira, "Defining control strategies for microgrids islanded operation," *IEEE Transactions on Power Systems*, vol. 21, no. 2, pp. 916–924, 2006.

[14] T. Ota, K. Mizuno, K. Yukita, H. Nakano, Y. Goto, and K. Ichiyanagi, "Study of load frequency control for a microgrid," in *Proceedings of the 2007 Australasian Universities Power Engineering Conference*, 2007, pp. 1–6.

[15] R. Scattolini, "Architectures for distributed and hierarchical model predictive control – a review," *Journal of Process Control*, vol. 19, no. 5, pp. 723–731, 2009.

[16] P. D. Christofides, R. Scattolini, D. Muñoz de la Pena, and J. Liu, "Distributed model predictive control – a tutorial review," *Computers & Chemical Engineering*, vol. 2451, pp. 21–41, 2013.

[17] A. Ulbig, M. Arnold, S. Chatzivasileiadis, and G. Andersson, "Framework for multiple time-scale cascaded MPC application in power systems," in *Proceedings of the 18th IFAC World Congress*, 2011.

[18] F. Kennel, D. Görges, and S. Liu, "Energy management for smart grids with electric vehicles based on hierarchical MPC," *IEEE Transactions on Industrial Informatics*, vol. 9, no. 3, pp. 1528–1537, 2013.

[19] G. Andersson, "Dynamics and control of electric power systems," Lecture Notes, Power System & High Voltage Laboratories, Department of Electrical and Computer Engineering, ETH Zurich, 2011, http:\\www.eeh.ee.ethz.ch\uploads\tx_ethstudies\DynCtrl_2011_part_1.pdf.

[20] D. Barcelli, A. Bemporad, and G. Ripaccioli, "Hierarchical multi-rate control design for constrained linear systems," in *Proceedings of the 49th IEEE Conference on Decision and Control*, 2010, pp. 5216–5221.

[21] B. Picasso, D. De Vito, R. Scattolini, and P. Colaneri, "An MPC approach to the design of two-layer hierarchical control systems," *Automatica*, vol. 46, no. 5, pp. 823–831, 2010.

[22] H. P. Williams, *Model Building in Mathematical Programming*, 4th ed. Chichester: John Wiley & Sons Ltd., 1999.

[23] M. Carrion and J. M. Arroyo, "A computationally efficient mixed-integer formulation for the thermal unit commitment problem," *IEEE Transactions on Power Systems*, vol. 21, no. 3, pp. 1371–1378, 2006.

[24] R. Gollmer, M. P. Nowak, W. Römisch, and R. Schultz, "Unit commitment in power generation – a basic model and some extensions," *Annals of Operations Research*, vol. 96, no. 1–4, pp. 167–189, 2000.